Meas. Sci. Technol. **20** (2009) 124007 (9pp) doi:10.1088/0957-0233/20/12/124007

Fabrication and performance characteristics of high-frequency micromachined bulk acoustic wave quartz resonator arrays

Ping Kao[1], **David Allara**[2,3] **and Srinivas Tadigadapa**[1,3]

[1] Department of Electrical Engineering, The Pennsylvania State University, University Park, PA 16802, USA
[2] Department of Chemistry, The Pennsylvania State University, University Park, PA 16802, USA
[3] Materials Research Institute, The Pennsylvania State University, University Park, PA 16802, USA

E-mail: dla3@psu.edu and sat10@psu.edu

Received 11 May 2009, in final form 1 July 2009
Published 26 October 2009
Online at stacks.iop.org/MST/20/124007

Abstract
This paper reviews the fabrication and performance of micromachined quartz resonator arrays. Using inductively coupled plasma etching techniques, we have successfully fabricated micromachined quartz resonator arrays with fundamental frequencies in the range of 25–85 MHz in an array format. These resonators have been experimentally evaluated for their performance in viscous (liquid) and viscoelastic (a biomolecular film in liquid) loading conditions. The paper discusses the ultimate sensitivity to mass and other properties of the adsorbates/contacting materials onto high-frequency quartz resonator surfaces. Measuring the frequency and Q-factor changes at the fundamental and third overtone of a 66 MHz resonator upon adsorption of immunoglobulin G (IgG) protein film on a hexadecanethiol functionalized surface, we were able to deduce: (i) the film thickness = 18 nm, (ii) density = 1040 kg m^{-3}, (iii) elastic modulus = 6.7 MPa and (iv) viscosity = 5.5 mPa s. Furthermore, from the adsorption isotherm for the IgG film, two different Langmuir equilibrium constants (K) were deduced. In the low-concentration region $K = 2.13 \times 10^8$ M^{-1} and in the high-concentration region $K = 6.53 \times 10^6$ M^{-1} were obtained. The thickness and density values obtained for IgG are consistent with the bilayer model predicted from interfacial packing of spherical protein molecules as a function of the molecular weight, and K values are consistent with earlier reported values for adsorption of IgG films. This is the first reporting of the elastic modulus and viscosity of IgG films in phosphate buffer solution.

Keywords: quartz resonators, viscoelastic properties, protein monolayers, immunoglobulin G, QCM, Langmuir isotherm

(Some figures in this article are in colour only in the electronic version)

Introduction

Bulk acoustic wave quartz resonators have been in steady use for a number of years as a convenient tool to determine mass loading of material layers at appropriate surfaces with layer thicknesses ranging well below the monolayer level. In spite of the experience gained with the wide use, the operating and design parameters of these devices have not been thoroughly explored to date, and there are opportunities to drive both the sensitivities and the measurement capabilities to new levels that can lead to new opportunities for improved operation in practical applications ranging from biomolecule

adsorption to exceedingly sensitive chemical sensors. In this paper, we describe, in detail, our recent experimental work with microfabricated high-frequency resonators operating in the transverse wave mode in which we have explored the determination of both the mass loading and viscoelastic response of adsorbed layers, including biomolecules. We show that by measuring the frequency and Q-factor changes at the first and third overtones, we are able to determine the thickness, density, viscosity and the elastic modulus of viscoelastic films in liquids. The paper is organized in terms of a review of the fundamental principles of operation of the resonators followed by the types of material parameters of adsorbed films that can be made, including mass, viscosity and viscoelastic response, and finally a presentation of our own results with micro resonator arrays.

General description of quartz shear mode resonators

A thickness shear mode quartz crystal resonator typically consists of a slab of thin, single-crystal, piezoelectric quartz, with very large lateral dimensions in comparison to its thickness, which is sandwiched between two metal electrodes. Application of a sinusoidal electric field using the electrodes sets up a shear wave through the thickness of the quartz, and under ideal boundary conditions where no other loading is present, the device exhibits a resonance behavior when the thickness of the quartz slab is half the wavelength of the shear acoustic wave. Thus the fundamental resonance frequency of a quartz resonator can simply be given by

$$f_0 = \frac{1}{2t_q}\sqrt{\frac{\mu_q}{\rho_q}}, \tag{1}$$

where t_q is the thickness of the quartz slab, μ_q and ρ_q are the shear modulus and density of quartz, respectively. One of the reasons for the widespread use of quartz resonators in frequency control applications is the exceptionally low phase noise obtained which allows for a precision of few parts in 10^{14} at optimal measurement times [1]. The phase noise is quantitatively specified in terms of the Q-factor defined as the half width at the full maximum of the resonance curve or in terms of an energy dissipation factor D, which is inversely proportional to the decay time constant and is also equal to the $1/Q$-factor.

The resonance frequency is significantly affected by any surface load placed on the quartz crystal including electrode metals. Loading on the resonator surface can be of three types: (i) pure elastic loads (rigid solids), (ii) pure viscous loads (liquids) and (iii) viscoelastic loads (polymers) and/or a combination of any of these. The interaction of the transverse shear wave with these loads has been treated using three fundamental approaches: (i) evaluation of electrical admittance characteristics upon mechanical perturbations on the resonators [2, 3], (ii) a continuum mechanics approach wherein the added material is modeled as a viscoelastic material with associated viscosity and elastic modulus [4, 5], (iii) the energy transfer model in which the quartz resonator and the deposited film are treated as a compound resonator, and energy balance methods are used to evaluate the perturbed characteristics of the resonator [6]. These approaches are based on a one-dimensional treatment of the problem since the lateral size of the resonators is typically much larger than the relevant dimensions such as the penetration depth of the acoustic waves in the direction perpendicular to the surface of the resonators.

Response of quartz resonator: elastic loading

The concept of mass measurement using a resonating quartz crystal was first presented by Sauerbrey [7]. For a resonator with a resonance frequency of $f_0(0)$ with no attached mass to it, the frequency change, Δf, upon addition of a rigid mass of small thickness in comparison to the quartz resonator thickness and under no-slip condition can be given by

$$\Delta f = -\left(\frac{2f_0^2(0)}{A\sqrt{\rho_q\mu_q}}\right)\Delta m = -\left(\frac{1}{t_q^2 A(2\rho_q)}\sqrt{\frac{\mu_q}{\rho_q}}\right)\Delta m, \tag{2}$$

where μ_q is the shear modulus of the crystal (2.947×10^{10} N m^{-2} for AT-cut quartz), ρ_q is the density of quartz (2.648×10^3 kg m^{-3}), t_q is the thickness of the quartz crystal, and A is the area of the electrode on the quartz crystal. The negative sign indicates a reduction in the resonance frequency upon mass loading. The most common commercially available quartz microbalances (QCMs) have a resonance frequency of 5–10 MHz. These typically consist of 25.4–12 mm diameter and 333–167 μm thick AT-cut quartz discs with gold electrodes on each face and exhibit a mass sensitivity of 17.7–4.42 ng cm^{-2} Hz, respectively. From equation (2) we can see that the mass sensitivity of the QCM can be increased by increasing its resonance frequency. Additionally, we can also conclude that as the area A of the resonator is made smaller, the change in frequency (Δf) for the same mass loading (Δm) increases. Thus as the quartz crystal resonators are made smaller, their absolute mass sensitivity increases. Based on empirical data, the smallest frequency noise in an AT-cut quartz resonator has been approximated to be $\sim 1.2 \times 10^{-20} f_0^2$ [8]. Thus the highest mass resolution that can be achieved by a given QCM can be calculated by dividing this expression by the mass–sensitivity factor in equation (2), i.e.,

$$\Delta m_{\text{ultimate}} = 0.6 \times 10^{-20} \times A\sqrt{\rho_q\mu_q} = 5.3 \times 10^{-15} A, \tag{3}$$

where $\Delta m_{\text{ultimate}}$ is given in grams, and area A is given in cm^2 units. Thus it is clear that decreasing the area of the resonator will improve the absolute mass sensitivity of the QCM. For instance, if the diameter of a resonator is reduced from 1 cm to 0.001 cm, an absolute mass resolution in the range of zeptograms (10^{-21} g) can be realized. At this size, micromachined quartz resonators can be viewed akin to the cantilever-type gravimetric sensors since the small active area can be better viewed as a platform more suitable for point mass loads than uniformly covering films with constant areal mass density.

In finite electrode sized resonators, energy trapping is necessary to maintain a high Q-factor and is determined by the effectiveness of the total internal reflection of vibrations at the edge of the electrodes to confine the acoustic energy to within this region only. For resonators where the diameter of the

electrodes is small compared to the quartz thickness, leakage of acoustic energy through the volume of the quartz increases considerably as vibrational energy reflection at the electrode edges becomes increasingly small. As a consequence, poor Q-factors are observed in such resonators.

On the other hand, for the effective suppression of the spurious modes, the rule-of-thumb thickness of quartz to electrode radius ratio is given by [9]

$$\Delta f_{\mathrm{pb}} < 0.744 f_{q0} \frac{1}{N^2} \left(\frac{t_q}{r_q}\right)^2, \tag{4}$$

where f_{q0} is the expected resonance frequency of the bare quartz crystal of thickness t_q before the mass loading due the electrodes, and Δf_{pb} is the plate back frequency, i.e. the frequency after the deposition of the top and bottom electrodes of radius r_q. This implies that as the quartz resonator thickness is reduced, the electrode diameter must also be reduced in order to effectively suppress spurious modes. Excessive decrease in the electrode diameter, however, will result in acoustic energy leakage and poor confinement of energy resulting in small Q-factors. These opposing requirements entail a design compromise. Our results show that for 50–70 MHz resonators with 100 nm of gold electrodes on both faces, the optimal electrode diameter ($2r_q$) to resonator thickness (x_q) ratio is ∼10–20. Large deviations from this value either way result in resonators with poor characteristics.

Response of quartz resonator: viscous loading

When used for applications such as biosensing and electrochemical studies, where one of the resonator surfaces is in contact with a liquid medium, the viscous drag effects need to be considered and now determine the ultimate device performance. Behavior of quartz resonators under purely viscous loading was first reported by Kanazawa and Gordon in 1985 [10]. Under such conditions, the fundamental mode QCM frequency shift is given by

$$\Delta f = -\frac{f_0^{3/2}}{\sqrt{\pi \rho_q \mu_q}} \sqrt{\rho_L \eta_L}, \tag{5}$$

where ρ_L and η_L are the viscosity and density of the liquid, respectively. The change in the quality factor ΔQ of the resonator under viscous loading conditions can be given by [9]

$$\Delta Q = \frac{\pi \rho_q \mu_q}{2\sqrt{\pi f_0 \rho_L \eta_L}} - \frac{\rho_q \mu_q^2}{2\pi f_0 \eta_q}. \tag{6}$$

For operation in liquids, the mass resolution of the QCM is modified and can be given as [11]

$$\mathrm{QCM}_{\mathrm{Resolution-Liquid}} = 5.64 \times 10^{-8} \frac{\sqrt{\rho_L \eta_L}}{\sqrt{f_0}} A, \tag{7}$$

where all quantities are specified in SI units. In the case of liquid operation, it is quite clear that a high-frequency resonator is likely to provide a higher mass resolution. However, often in liquid applications, we are interested in measuring viscosity and density changes in liquid rather than mass changes.

In order to calculate the ultimate density/viscosity resolution of a quartz resonator, we begin by noting that the smallest frequency variation that can be detected in the presence of noise is given by the expression

$$\Delta f(\tau) = 2 \times 10^{-7} \frac{f_0}{Q_{\max}}, \tag{8}$$

where $Q_{\max} \approx \omega_0 L_q / R_L$ is the maximum Q-factor that can be achieved in a resonator loaded with liquid on one of its faces. L_q is the motional inductance of the quartz resonator, $\omega_0 = 2\pi f_0$, and R_L is the motional resistance arising due to the liquid in contact with the quartz resonator. Using the expression for R_L [12]

$$R_L = \frac{\omega_0 L_q}{\pi} \left(\frac{4\pi f_0 \rho_L \eta_L}{\mu_q \rho_q}\right)^{1/2}, \tag{9}$$

$Q_{\max}$ can be written as

$$Q_{\max} = \pi \left(\frac{\mu_q \rho_q}{4\pi f_0 \rho_L \eta_L}\right)^{1/2}. \tag{10}$$

Expressing Δf as a function of liquid density and viscosity, we can write

$$\Delta(\Delta f) = \frac{\mathrm{d}(\Delta f)}{\mathrm{d}\rho_L} \Delta\rho_L + \frac{\mathrm{d}(\Delta f)}{\mathrm{d}\eta_L} \Delta\eta_L. \tag{11}$$

Substituting equation (8) in equation (10) for $\Delta(\Delta f)$, and using equation (5) for the functional dependence of Δf on the density and viscosity of the liquid, we can write

$$\frac{\Delta\eta_L}{\eta_L} + \frac{\Delta\rho_L}{\rho_L} = 4 \times 10^{-7} \tag{12}$$

for the ultimate resolution of viscosity and density using a QCM. Since most liquid experiments are accompanied by simultaneous changes in the density and the viscosity of the liquid, equation (12) gives the combined minimum resolution in both parameters.

Furthermore, in liquid medium applications, the shear wave rapidly damps out as it travels through the thickness of the liquid, and consequently the QCM typically samples a layer of thickness equivalent to the decay length $\delta = (\eta_L/\pi\rho_L f_0)^{0.5}$ [13]. For a commercial 5 MHz QCM, the typical decay length in water is ∼250 nm, which is large in comparison to the thickness of molecular or even polymer and biomolecular (e.g., proteins) films which can be in a thickness range of 10–50 nm. As a result, a commercial QCM not only samples the adsorbed film but is also significantly affected by the viscous liquid layer above it. Small changes in the viscoelastic properties of adsorbed layers are often masked by the viscous effects from the liquid overlayer. However, if the QCM thickness is decreased, its fundamental resonance frequency increases inversely as a function of the thickness of quartz and thus the decay length in liquid also decreases consequently. For example, if the thickness of a quartz resonator is decreased from 330 μm (commercial 5 MHz resonator) to 24 μm (miniaturized 66–69 MHz resonator), the decay length in water is reduced to ∼68 nm. These factors are critical to the improved abilities of miniaturized devices to probing viscoelastic characteristics of adsorbed layers compared to standard commercial QCMs.

Response of quartz resonator: viscoelastic loading in liquid ambient

The QCM frequency shift resulting from the deposition of a viscoelastic layer in a viscous liquid ambient can be analyzed using the continuum mechanics approach, for example as developed by Kasemo and coworkers [5]. In order to model this situation, the QCM surface is considered to be in intimate contact with a layer of the continuous viscoelastic slab with an infinitely thick Newtonian liquid overlayer on one of its surfaces. Under the assumption that the thickness of the bulk liquid layer is much larger than the decay length of the acoustic wave in the liquid, the frequency, Q-factor and dissipation factor changes with respect to liquid loading conditions can then be written as

$$\Delta f \approx -\frac{1}{2\pi\rho_q t_q}\left(t_{\text{visc}}\rho_{\text{visc}}\omega - 2t_{\text{visc}}\left(\frac{\eta_L}{\delta_L}\right)^2\frac{\eta_{\text{visc}}\omega^2}{\mu_{\text{visc}}^2+\omega^2\eta_{\text{visc}}^2}\right), \tag{13}$$

$$\Delta Q \approx -2\pi f_0\rho_q t_q\frac{\left(2t_{\text{visc}}\frac{\mu_{\text{visc}}\omega}{\mu_{\text{visc}}^2+\omega^2\eta_{\text{visc}}^2}\right)}{\left[1+\left(2t_{\text{visc}}\left(\frac{\eta_L}{\delta_L}\right)\frac{\mu_{\text{visc}}\omega}{\mu_{\text{visc}}^2+\omega^2\eta_{\text{visc}}^2}\right)\right]}, \tag{14}$$

$$\Delta D \approx \frac{1}{2\pi f_0\rho_q t_q}\left(2t_{\text{visc}}\left(\frac{\eta_{\text{visc}}}{\delta_{\text{visc}}}\right)^2\frac{\mu_{\text{visc}}\omega}{\mu_{\text{visc}}^2+\omega^2\eta_{\text{visc}}^2}\right), \tag{15}$$

where μ_{visc}, η_{visc} and ρ_{visc} are the elastic modulus, viscosity and density of the viscoelastic layer respectively, and t_{visc} is its thickness and δ_L is the penetration depth of the acoustic wave in the liquid.

Description and fabrication of micromachined quartz resonator arrays

Figure 1 shows the schematic illustration of the process flow for the fabrication of micromachined quartz resonator arrays. On a 100 μm thick, 1" diameter polished AT-cut quartz crystals (figure 1(a)), a 20/100 nm thick Cr/Au seed layer was deposited. 10–12 μm thick nickel was electroplated with a patterned photoresist as the mask (figure 1(b)). 75 μm deep circular pits with a diameter of 1 mm were etched using reactive ion etching in the SF_6+Ar plasma (figure 1(c)). After completion of the etch, the remaining nickel hard mask was stripped in aqua regia solution (figure 1(d)). This was followed by the deposition and patterning of the bottom side 20/150 nm thick Cr/Au electrodes for individual resonator pixels (figure 1(e)). Finally, 20/80 nm thick Cr/Au top-side electrodes were evaporated and patterned to complete the device (figure 1(f)). The creation of an abrupt step in the quartz substrate for each pixel acoustically and energetically isolates each of these for the shear mode operation [14, 15]. Each resonator is individually addressed through backside (etched side) electrodes, which are extended to the rim of the sensor array chip. The top electrode is common to all the pixels of the array. In order to effectively confine the acoustic energy in each pixel, the pixel thickness to diameter of the electrodes ratio has been carefully optimized [16]. The mounting and packaging of the array and the interconnection

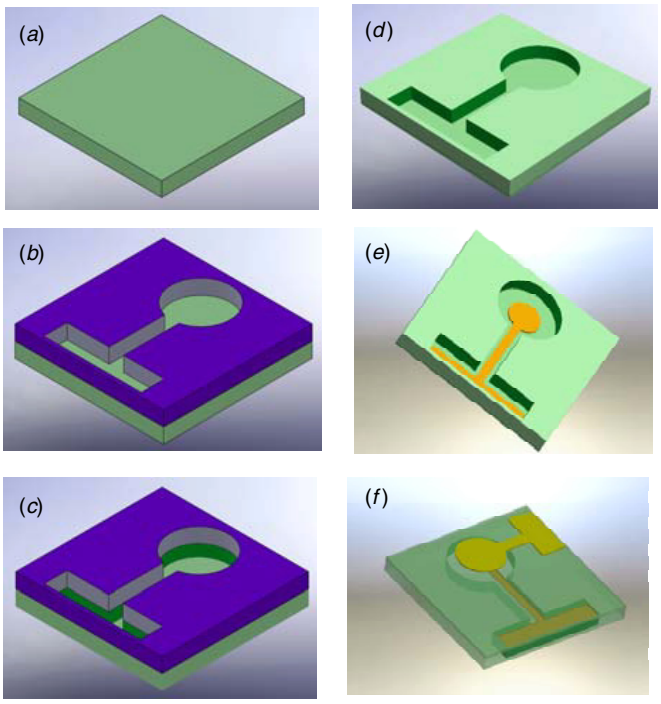

Figure 1. Schematic illustration of the fabrication of micromachined quartz resonator array. (a) 100 μm thick AT-cut quartz substrate, (b) electroplating of the patterned nickel layer, (c) inductively coupled reactive ion etching of quartz, (d) stripping of the nickel hard mask, (e) deposition and patterning of the Cr/Au backside electrode and (f) deposition and patterning of the Cr/Au front-side common electrode.

were also carefully optimized to maintain a high-quality factor of the resonators. The resonance frequency is determined by the thickness of the pixel. Figure 1(a) shows a schematic illustration of the fabricated resonator array and figure 1(b) shows the packaged device placed on the liquid test cell. As shown in figure 1(b), a dual in-line ceramic package was modified with a square hole cut in it for the mounting of the array. The array was attached to the package using room-temperature vulcanized silicone. For the fabricated 25 μm thick pixel, the fundamental resonance frequency is expected to be 66.72 MHz. Fabricated devices were mounted in a specially designed Teflon test cell capable of liquid testing experiments.

Performance of micromachined quartz resonators

All measurements reported in this work were measured using Agilent 4294A and Agilent 4395A impedance analyzers. Ceramic dual in-line packages similar to those used for the packaging of the QCM device were modified to provide open- and short-circuit compensation fixtures for accurate calibration of the QCM. A 100 Ω resistor was used to simulate the load for compensation in the 1 kHz to 250 MHz frequency range. The impedance analyzer was set up to simultaneously measure the impedance magnitude and phase angle as a function of frequency. All measurements were carried out inside a 4″ × 5″ × 3″ aluminum die-cast temperature controlled box to prevent RF interference and the temperature set at

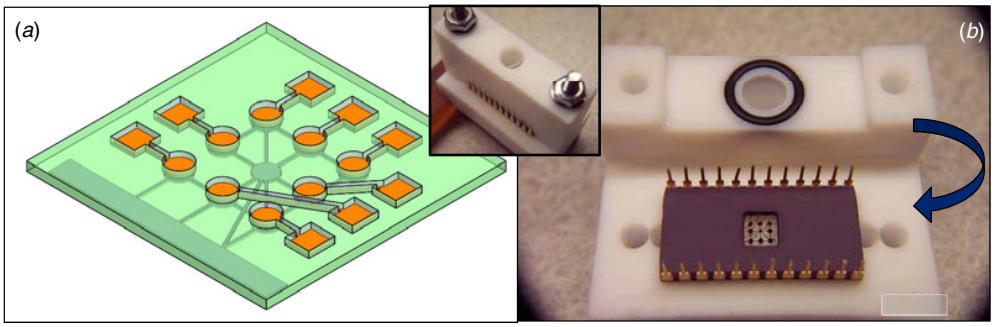

Figure 2. (*a*) Schematic illustration of the fabricated resonator array from the backside (etched side) showing eight resonators in the array. (*b*) An optical picture of the packaged resonator array in a modified ceramic dual in-line 24-pin package placed on the Teflon test cell. The inset shows the assembled test cell filled with ethanol.

Table 1. Summary of the typical resonance parameters of the micromachined resonator in air.

C_0 (static capacitance) (pF)	1.982 74	2.563 15
C_m (motional capacitance) (fF)	1.2448	2.346 272
L_m (motional inductance) (mH)	4.406 89	1.446 98
R_m (motional resistance) (Ω)	45.8688	16.1715
f_s (series resonance) (MHz)	67.957 201	86.345 250
f_p (parallel resonance) (MHz)	67.978 848	86.377 301
Q-factor	41 023.26	48 543

22.5 (±0.1) °C. For viscoelastic measurements, a single pixel from the array was chosen for all the measurements reported. All measurements were performed in air, water, phosphate buffer solution using the Teflon test cells shown in figure 2(*b*).

Admittance characteristics

Figure 3 shows the at-resonance admittance (Y) curve for the 8 pixels of the array in air. All the fabricated pixels show the expected admittance characteristics. The motional resistance and series resonance frequency were determined directly from the inverse of the maximum and peak of the real part of the admittance, respectively, and are listed in the graphs in figure 3 for each pixels in the chip. The average resonance frequency for the array is 70.103 ± 2.480 MHz. Table 1 lists the typical resonance parameters obtained for the micromachined quartz resonators.

Cross-talk measurement

To measure the cross-talk between pixels, the impedance analyzer was programmed to scan a narrow band of frequency, spanning the resonance frequency of the resonators. An HP-4195A spectrum analyzer was used to measure the signal strength when connected directly to the pixel being driven and at several of the nearby pixels on the sensor array sequentially. The experiment was performed with the top side of the resonator exposed to air and water ambient. Measurement of the direct output of the signal generator gave a signal output of 88 dBm against the output from one of the neighboring pixel of ∼58 dBm implying an isolation of ∼30 dB at 62 MHz frequency in both air and water environment conditions [15].

Water–glycerol calibration experiment

Next the operation of the micromachined QCM array was carefully investigated in liquids using water and water–glycerol mixtures of various concentrations. Table 2 shows the typical resonance frequency and Q-factors obtained for the various resonators in air and water. As can be seen, the micromachined resonators exhibit a Q-factor, which is very close to the predicted $Q_{\max}$ from equation (10), indicating that the resonator is primarily damped by viscous loading of water. Water and glycerol are miscible liquids with pure-form densities of 0.998 21 g cm^{-3} and 1.2613 g cm^{-3}, and viscosities of 1.005 mPa s and 1499 mPa s at 20 °C respectively. The behavior of the QCM under viscous (liquid) loading conditions is given by equation (5). The frequency decrease is linearly proportional to the square root of the viscosity–density product of the liquid loading atop the QCM electrode surface. Figure 4 shows the frequency change for three different sensors, with fundamental resonance frequencies of ∼25, 66 and 83 MHz and at the third overtone of the 66 MHz resonator, as the resonator surfaces were exposed to different concentrations of the water–glycerol mixtures. The results clearly show the expected linear dependence for the QCM frequency change with the square root of the liquid density–viscosity product at the fundamental as well as the third overtones and agree well with the expected behavior predicted using equation (5). The sensitivity with respect to liquid $(\rho_L \eta_L)^{1/2}$ clearly scales as $f_0^{3/2}$ at the fundamental frequency and as $f_0^{1/2}$ at the third overtone in comparison to the fundamental frequency.

Adsorption characteristics of immunoglobulin G on the QCM surface

The QCM gold electrodes were first functionalized to produce a highly hydrophobic surface by chemisoprtion of hexadecanethiol (HD) to form a densely packed self-assembled monolayer (SAM). Immunoglobulin G (IgG) protein was then adsorbed on these hydrophobic surfaces to form a uniform viscoelastic layer.

Immunoglobulin G from rabbit serum (Sigma Aldrich), 2.4 mg ml^{-1} rabbit anti-human IgG, $F_c\gamma$, unconjugated (Pierce Biotechnology) and glycerol (JT Baker) were used directly. The phosphate buffer solution (PBS) was made by dissolving

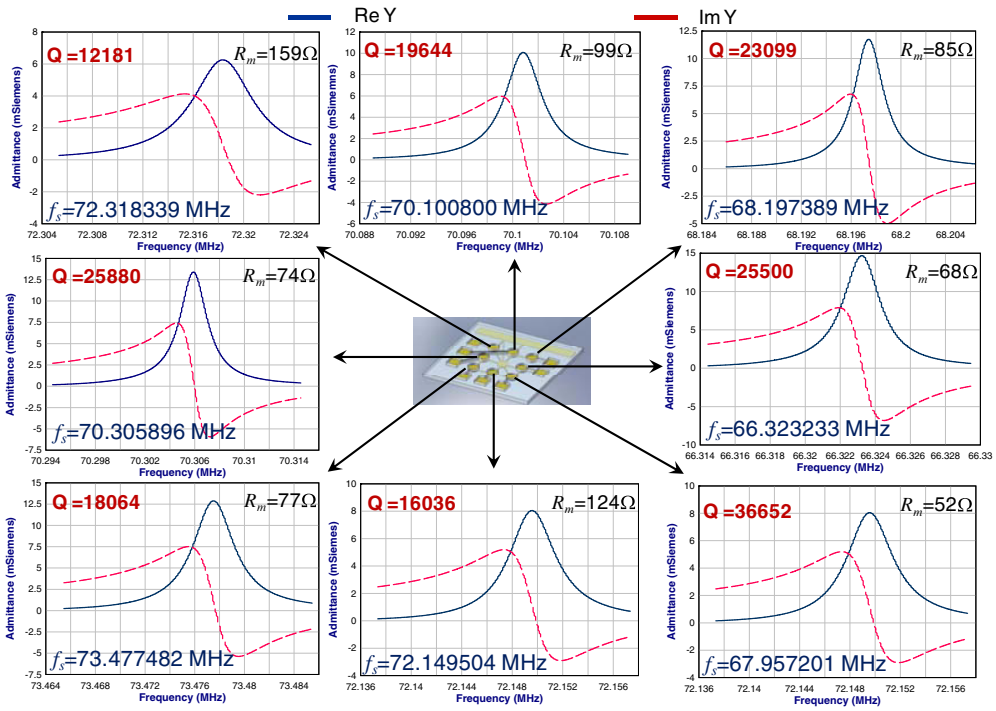

Figure 3. Admittance characteristics of the 8 pixels in the resonator array. An average frequency of 70.103 ± 2.480 MHz was determined across the array. The average Q-factor for the array was 22 132 with an average motional resistance of 92.6 Ω.

Table 2. A list of the fundamental frequencies and Q-factors in air and in water of the commercial (333 μm) thick QCM and the micromachined QCM. For all the resonators, the obtained Q-factors are close to the limit of maximum Q-factor (Q_{max}) that can be obtained in water (shown in parenthesis).

QCM thickness	In air		In water	
(μm)	Frequency (MHz)	Q-factor	Frequency (MHz)	Q-factor
333	5.008 854	170 962	5.008 091	3048 (3498)
26	62.926 070	20 745	62.895 670	903 (987)
18	83.036 181	45 916	82.987 985	847 (859)

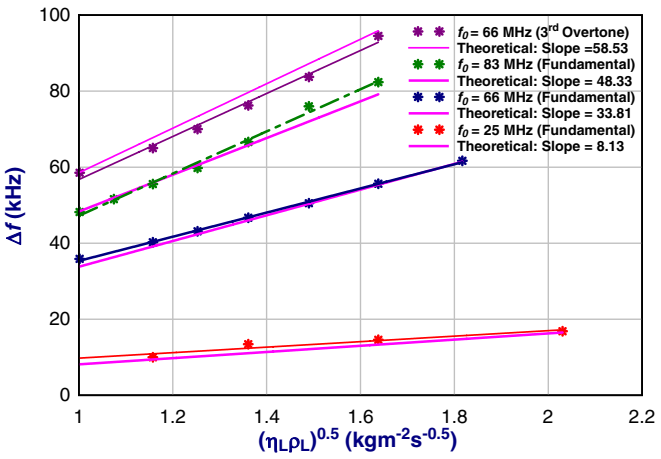

Figure 4. The expected linear dependence of the frequency change as a function of the square root of the liquid viscosity–density product for micromachined resonators with fundamental resonance at 25, 66 and 83 MHz and at the third overtone of the 66 MHz resonator.

phosphate buffered saline powder (Sigma Aldrich) into 18 MΩ cm deionized water (Millipore Milli-Q system; Barnstead international). 0.005 mg ml^{-1}, 0.05 mg ml^{-1} and 0.5 mg ml^{-1} IgG concentration solutions were prepared by diluting a 5 mg ml^{-1} stock solution. Serial IgG concentration solutions in the test cell were made by continuously adding higher concentration solution.

The micromachined QCM was cleaned by three cycles of exposure to UV ozone, each 30 min long, followed by thorough rinsing with ethanol and immersion in ethanol for 1 h. Finally, the electrodes were exposed to 1 mM hexadecanethiol solution in ethanol for 48 h. This step functionalized the gold electrodes with a high-density methyl-terminated SAM. 198 μl PBS solution was delivered to the electrode surface, and the QCM was allowed to stabilize for 1 h to a constant frequency. This was followed by the sequential injection of increasing concentration protein solutions.

The real-time shift in the resonance frequency and quality factor of the resonator as various concentrations of IgG are sequentially added is shown in figure 5(*a*). A plot of the resonance frequency shifts versus IgG solution concentration for adsorption on the HD-SAM coated gold electrodes is shown in figure 5(*b*). A similar shaped curve was obtained in an earlier study on the adsorption of human serum albumin

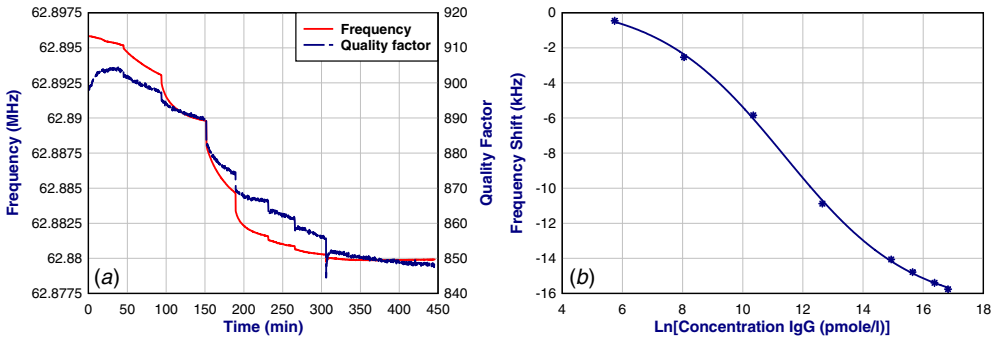

Figure 5. (*a*) The real-time frequency and quality factor shift as increasing concentrations of IgG are placed onto the QCM surface. (*b*) Shift of the QCM resonance frequency as a function of the natural logarithm of the concentration of IgG in solution for adsorption on a HD-SAM gold electrode.

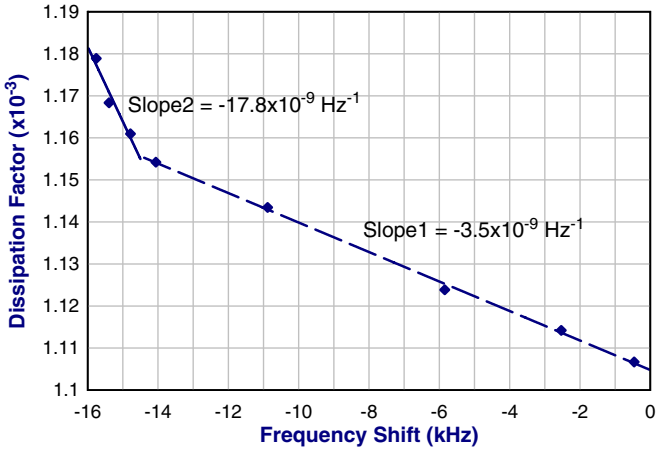

Figure 6. Change in the dissipation factor (ΔD) plotted against the change in the resonance frequency (Δf) for different concentrations of IgG protein solutions. Two distinct slopes are seen; namely, in the low-concentration region with a value of 3.5×10^{-9} Hz^{-1} and in the high-concentration region with a value of 17.8×10^{-9} Hz^{-1}. The adsorbed film is expected to be less rigid and more viscous in the high-concentration region.

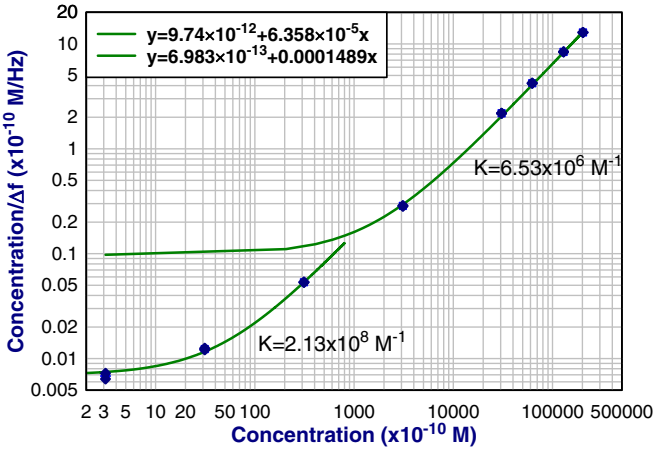

Figure 7. A Langmuir model plot of adsorbed IgG mass, represented by Δf, versus IgG concentration for the entire concentration range tested. The solid line is a linear fit to the data, consistent with a Langmuir behavior. Two distinct sloped straight lines can be fitted to the low- and high-concentration region of the data. Using these slopes, the Langmuir equilibrium constant K can be calculated in the concentration regions. The spread in the data indicates the error in the measurements which can only be seen in the low-concentration region.

(HSA) on HD SAM using a 62 MHz micromachined QCM [16]. Both sets of data show very close fits with high ($>$0.99) R^2 values to a sigmoidal function. The curves differ, however, in that the full span of the frequency shift over similar concentration ranges of the two different molecules was ∼6.8 kHz and ∼16 kHz for HSA and IgG molecules, respectively.

In figure 6, the observed change in the dissipation factor ΔD is plotted against the change in frequency Δf for the various concentrations of IgG. The dissipation factor was calculated by taking the inverse of the experimentally measured Q-factor under each loading condition. The slope reveals the rigidity of the adsorbed layer. A low value of $\Delta D/\Delta f$ indicates a highly rigid, low dissipation layer, and conversely a high $\Delta D/\Delta f$ value indicates a soft, dissipative film. The adsorption of IgG on the HD-SAM surface shows two different values for the slope $\Delta D/\Delta f$ (figure 6). In the low-concentration region, a value of 3.5×10^{-9} Hz^{-1} is obtained indicative of a rigid adsorbed film [17]. However, in the high-concentration region, nearly five times higher value of 17.8×10^{-9} Hz^{-1} is obtained showing that the film has become less rigid.

The appearance of more than one slope has also been reported by Zhou *et al* [18] and can be interpreted as arising due to the conformational changes expected at high concentrations. As we will discuss later, IgG is expected to adsorb on a hydrophobic surface as a bilayer [19]. It is possible that the low-concentration slope is associated with the molecular adsorption on the surface of the QCM until a monolayer is formed. Upon the adsorption of a monolayer, the process is expected to proceed toward the formation of the bilayer which might be associated with further conformational changes in the adsorbed film leading to the increased viscous behavior. Next, we analyze this result in terms of the viscoelastic model and its significance in terms of the currently known protein adsorption models and theory.

Assuming a limiting coverage of a uniform layer IgG adsorption behavior can be tested for a fit to a Langmuir isotherm. Figure 7 is a log–log plot of $C/\Delta f$ versus C. Ideally, a linear relationship is expected from the slope and intercept of

Table 3. Measured and theoretically predicted frequency and Q-factor shifts for the 66 MHz resonator. Measuring the frequency shift and Q-factor at the first and third modes allows for unique determination of the viscoelastic properties of the IgG film.

IgG film parameters used: $t_{IgG} = 18$ nm, $\rho_{IgG} = 1040$ kg m^{-3} $\mu_{IgG} = 6.7$ MPa, $\eta_{IgG} = 5.5$ mPa s	Frequency shift (kHz)		Q-factor shift	
	Measured	Theory	Measured	Theory
First mode	15.75	16.48	54	54
Third mode	48.39	47.20	254	258

which the Langmuir equilibrium constant can be calculated. However, as seen in the graph, two different values of the equilibrium constant are obtained. The low-concentration behavior gives a value of $K = 2.13 \times 10^8$ M^{-1} whereas at high concentrations a value of $K = 6.53 \times 10^6$ M^{-1} is obtained. Similar observation was found in our earlier work on HSA adsorption and has been reported for the adsorption for IgG on protein A [16, 20].

For a further discussion on the viscoelastic effects, we analyzed the results in the saturation region where we expect the IgG film to have uniformly adsorbed over the entire QCM electrode layer. Given the thin (∼2 nm), chemically attached, dense nature of the HD-SAM layer, it can be accurately considered as a rigid extension of the electrode. The adsorbed IgG layer on the other hand is only attached to the HD-SAM surface via van der Waals' forces with each molecule surrounded by water and in contact with the phosphate buffered saline solution (PBS) [19]. Thus the IgG layer is considered to be viscoelastic in nature whereas the surrounding PBS solution, containing only a very low volume fraction of protein molecules, can be represented as a Newtonian fluid. Furthermore, we have measured the change in frequency as well as the change in the Q-factor at the fundamental and third mode of the resonator upon adsorption of IgG. Experimental results show a decrease of 15.755 kHz in the frequency and 54.8 in the Q-factor at the fundamental mode of operation and a decrease of 48.393 kHz in frequency and 254.8 in the Q-factor at the third overtone. Using expressions given by equations (13) and (14), the expected frequency and Q-factor changes can be calculated. In order to model the system, the thickness, density, elastic modulus and viscosity of the IgG layer were considered as parameters and varied to fit to the experimental data. As shown in table 3, we were able to obtain a very good match between the observed and expected Δf and ΔQ for IgG parameters of $t_{IgG} = 18$ nm, $\rho_{IgG} = 1040$ kg m^{-3}, $\mu_{IgG} = 6.7 \times 10^6$ Pa and $\eta_{IgG} = 0.0055$ Pa s.

The protein adsorption model given by Krishnan *et al* shows that the interfacial packing of spherical protein molecules is a function of molecular weight [21]. The number of layers, the size of protein molecules and the mass of protein adsorbed onto the interphase can be calculated as long as the molecular weight of protein is given. Applying this model to IgG protein adsorption onto a hydrophobic surface, it can be concluded that the IgG will form a bilayered structure with a thickness of 9.4 nm per layer (or a total thickness of 18.8 nm for the bilayer) and a density of 1017 kg m^{-3} per layer [21]. These values of thickness and density of IgG agree very well with the values extracted from the first and third mode $\Delta f - \Delta Q$ changes upon IgG adsorption onto the QCM surface. To the best of our knowledge, this is the first report of the elastic modulus and viscosity of the IgG protein layer.

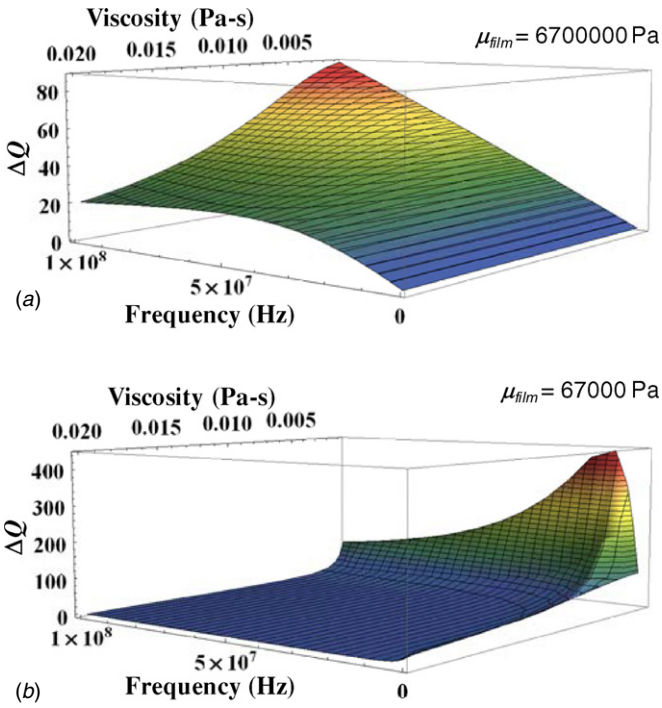

Figure 8. The parametric dependence of ΔQ value as a function of the resonator frequency and viscosity of the adsorbed film for two different values of the elastic modulus of the film of 67 kPa and 6.7 MPa. In this simulation, the film thickness was assumed to be 18 nm, and its density as 1.04 g cm^{-3}.

Finally, to confirm that the observed effects are due to the adsorption of the IgG layer, the resonance frequency and Q-factor were monitored upon the addition of anti-IgG. Prior to the addition of anti-IgG solution, the QCM surface was rinsed ten times with PBS solution, rinsed thoroughly and gently dried under a filtered N_2 stream. 200 μl PBS solution was first added for stabilization of the QCM and was followed by the injection of 110 μl anti-IgG solution. An additional frequency decrease of 9.275 kHz was obtained confirming the presence of the IgG layer on the QCM electrode.

In conclusion, we have demonstrated that high-frequency resonators are especially suited for monitoring small changes in the viscoelastic loading in films adsorbed on their surface. Figure 8 shows the parametric dependence of the ΔQ value as a function of the resonator frequency and viscosity of the adsorbed film for two different values of the elastic modulus of the film of 67 kPa and 6.7 MPa. It can clearly be seen

that the higher-frequency resonators will resolve the Q-factor better than lower-frequency resonators for most viscoelastic loads except when the elastic modulus of the films is very low. A large variation in the Q-factor and the frequency for small changes in the viscoelastic properties of the adsorbed film is highly desirable for the accurate determination of the material properties of the films and for the observation of conformational changes in these nanometer thin films. Lastly, micromachined QCM resonators also show a smaller noise level with regards to the dissipation factor. Under identical IgG loading condition, we were able to obtain a dissipation noise of 5.8×10^{-7} as compared to the reported value of 7×10^{-7} for the commercial resonator [18]. This implies that the micromachined QCM exhibits a much larger signal-to-noise ratio for this application.

Conclusions

In this paper, we have reviewed the overall performance of 65–85 MHz micromachined resonator arrays. The presented data show that the devices can be fabricated as arrays and readily packaged for testing in liquids. High Q-factors in the range of 25 000–50 000 have been obtained for the resonators. For pure elastic material loading in air or vacuum conditions, ideal analysis predicts that the signal-to-noise ratio is unaffected by increasing the frequency of the QCM devices. In liquid ambient, the ideal signal-to-noise ratio improves as $f_0^{1/2}$ for elastic loading but more importantly the QCM is also very sensitive to variations in density and viscosity of the liquids. The high stability and inherent low noise of quartz crystals allow for an unprecedented resolution of one part in 10 million for density/viscosity variations. However, without measuring the frequency decrease at overtone frequencies, it is not possible to identify individual variations in the density and viscosity. By measuring the frequency and dissipation factor changes at fundamental and third overtone, we were able to accurately determine the thickness, density, elastic modulus and viscosity of the IgG layer adsorbed on the hexadecane thiol functionalized QCM surface.

Acknowledgments

The authors acknowledge partial financial support from the NSF funded PSU Center for Nanoscale Science (MRSEC DMR-0080019) and the use of facilities at the PSU Site of the NSF NNIN under Agreement 0335765. The authors also acknowledge financial support from the US Army Research Office (grant # W911NF-07-1-0327).

References

[1] Walls F L and Vig J R 1995 Fundamental limits on the frequency stabilities of crystal oscillators *IEEE Trans. Ultrason. Ferroelectr. Freq. Control* **42** 576–89

[2] Bandey H L, Martin S J, Cernosek R W and Hillman A R 1999 Modeling the responses of thickness-shear mode resonators under various loading conditions *Anal. Chem.* **71** 2205–14

[3] Lucklum R and Hauptmann P 2000 The quartz crystal microbalance: mass sensitivity, viscoelasticity and acoustic amplification *Sensors Actuators* B **70** 30–6

[4] Rodahl M and Kasemo B 1996 On the measurement of thin liquid overlayers with the quartz-crystal microbalance *Sensors Actuators* A **54** 448–56

[5] Voinova M V, Rodahl M, Jonson M and Kasemo B 1999 Viscoelastic acoustic response of layered polymer films at fluid-solid interfaces: continuum mechanics approach *Phys. Scr.* **59** 391

[6] Mecea V and Bucur R V 1979 The mechanism of the interaction of thin films with resonating quartz crystal substrates: the energy transfer model *Thin Solid Films* **60** 73–84

[7] Sauerbrey G 1959 Verwendung von Schwingquarzen zur Wagung dunner Schichten und zur Mikrowagung *Z. Phys.* **155** 206–22

[8] Vig J R, Filler R L and Kim Y 1996 Uncooled IR imaging array based on quartz microresonators *J. Microelectromech. Syst.* **5** 131–7

[9] Lucklum R and Eichelbaum F 2007 Interface circuits for QCM sensors *Piezoelectric Sensors* vol 5 ed C Steinem and A Janshoff (Berlin: Springer) pp 3–47

[10] Kanazawa K K and Gordon J G 1985 Frequency of a quartz microbalance in contact with liquid *Anal. Chem.* **57** 1770–1

[11] Rodriguez-Pardo L, Farina J, Gabrielli C, Perrot H and Brendel R 2004 Resolution in quartz crystal oscillator circuits for high sensitivity microbalance sensors in damping media *Sensors Actuators* B **103** 318–24

[12] Martin S J, Granstaff V E and Frye G C 1991 Characterization of a quartz crystal microbalance with simultaneous mass and liquid loading *Anal. Chem.* **63** 2272–81

[13] Janshoff A, Galla H-J and Steinem C 2000 Piezoelectric mass sensing devices as biosensors—an alternative to optical biosensors? *Angew. Chem., Int. Ed. Engl.* **39** 4004–32

[14] Rabe J, Buttgenbach S, Schroder J and Hauptmann P 2003 Monolithic miniaturized quartz microbalance array and its application to chemical sensor systems for liquids *IEEE Sensors J.* **3** 361

[15] Kao P, Doerner S, Schneider T, Allara D, Hauptmann P and Tadigadapa S 2009 A micromachined quartz resonator array for biosensing applications *J. Microelectromech. Syst.* **18** 522–30

[16] Kao P, Patwardhan A, Allara D and Tadigadapa S 2008 Human serum albumin adsorption study on 62-MHz miniaturized quartz gravimetric sensors *Anal. Chem.* **80** 5930–6

[17] Hook F, Rodahl M, Brzezinski P and Kasemo B 1998 Energy dissipation kinetics for protein and antibody-antigen adsorption under shear oscillation on a quartz crystal microbalance *Langmuir* **14** 729–34

[18] Zhou C, Friedt J-M, Angelova A, Choi K-H, Laureyn W, Frederix F, Francis L A, Campitelli A, Engelborghs Y and Borghs G 2004 Human immunoglobulin adsorption investigated by means of quartz crystal microbalance dissipation, atomic force microscopy, surface acoustic wave, and surface plasmon resonance techniques *Langmuir* **20** 5870–8

[19] Krishnan A, Liu Y-H, Cha P, Allara D and Vogler E A 2006 Interfacial energetics of globular–blood protein adsorption to a hydrophobic interface from aqueous-buffer solution *J. R. Soc. Interface* **3** 283

[20] Ogi H, Motohisa K, Hatanaka K, Ohmori T, Hirao M and Nishiyama M 2007 Concentration dependence of IgG-protein A affinity studied by wireless-electrodeless QCM *Biosens. Bioelectron.* **22** 3238–42

[21] Krishnan A, Siedlecki C A and Vogler E A 2003 Traube-rule interpretation of protein adsorption at the liquid–vapor interface *Langmuir* **19** 10342–52